Optical Properties of MEH-PPV Conjugated Polymer Covered by Silica Nanoshells

G. A. M. Sáfar,[1,2] F. A. C. Oliveira,[2] L. A. Cury,[2] A. Righi,[2] P. L. M. Barbosa,[2] P. Dieudonné,[3] F. S. Lameiras[1]

[1]*Centro de Desenvolvimento da Tecnologia Nuclear—CDTN/CNEN, Campus Universitário, 30123-970, Belo Horizonte, Minas Gerais, Brazil*
[2]*Departamento de Física, Instituto de Ciências Exatas, Universidade Federal de Minas Gerais, Campus Universitário, 30123-970 Belo Horizonte, Minas Gerais, Brazil*
[3]*Laboratoire des Colloïdes, Verres, et Nanomatériaux, Université de Montpellier 2, Pl: E. Bataillon, 34095 Montpellier, France*

Received 15 March 2006; accepted 25 June 2006
DOI 10.1002/app.24987
Published online in Wiley InterScience (www.interscience.wiley.com).

ABSTRACT: Poly [2-methoxy-5-(2′-ethyl-hexyloxy)-1,4-phenylene vinylene] (MEH-PPV) covered by nanostructured silica shells were synthesized via sol–gel process and investigated after freeze-drying and heat-drying in vacuum. The freeze-dried sample consists of a light pink powder while the heat-dried sample presents a redder coarse-grained material. The freeze-dried sample was analyzed using small angle X-ray scattering (SAXS). Both samples were analyzed using photoluminescence (PL) and Raman spectroscopy at room temperature. The PL spectra presented relatively large red shifts compared with that of the MEH-PPV in tetrahydrofuran solution, which was taken as a reference sample. The energy shifts observed in the PL and Raman spectra strongly support an explanation based on denser packing conditions inside the nanostructured silica shells, which can effectively lead the polymer molecules to a higher interchain interaction via aggregate sites. J Appl Polym Sci 102: 5620–5626, 2006

Key words: light scattering; luminescence; conjugated polymers; particle size distribution; gels

INTRODUCTION

Conjugated polymers are remarkable materials because of their plastic and semiconducting properties, making them very useful for electrooptical applications.[1–3] In addition, the easy manufacturing of polymer solutions enables the production of composite materials that aggregate the polymer properties with those of the additional component, creating new materials with different and peculiar properties. Thus, hybrid composites involving organic and inorganic materials have been extensively investigated in attempts to achieve better optical and electrical characteristics. For example, the mixing of insulating oxide nanoparticles in polymer films to promote the increase of the emission efficiency in organic light emitting diodes and laser structures has been studied.[4,5] In addition, incorporation of cadmium selenide, C_{60} derivatives, and titanium dioxide into a photoconducting polymer can result in improved efficiency of photovoltaic devices.[6–11] Metal nanoparticles were also used to change the optical properties of new composite polymer materials.[12,13] An interesting method to prepare composite polymer materials is the use of porous silica (PS),[14–18] which is in fact the aim of the optical investigation reported here. In a previous work,[14] PS incorporated to the polymer matrix did not seem to effectively affect the optical properties of PPV/PS composite films. Only small changes were observed in the shape of the photoluminescence (PL) spectra at different PS concentrations, which were in part explained by the presence of residual oxygen introduced by the silicon grains. For PPV–silica nanocomposite thin films,[15] a blue shift of the pure electronic transition PL peak has been observed with the increase in volume fraction of silica. The blue shift was mainly attributed to a reduction of the effective conjugation length of the polymer. Small effects, mainly in the shape of the absorption and the PL spectra, were observed in composite films of PPV/metal-coated silica nanoparticles.[16] The major effect of metal-coated silica nanoparticles was to retard the photooxidation process in PPV nanocomposite films.

Thus, to our knowledge, the previous investigations have not yet shown significant effects on the optical properties of silica nanoparticles/conjugated polymer composites, in comparison to those reported here. In

Correspondence to: G. A. M. Sáfar (gamsafar@yahoo.com.br).
Contract grant sponsors: CNPq, FAPEMIG, Nanoscience Millennium Project.

this work, poly[2-methoxy-5-(2′-ethyl-hexyloxy)-1,4-phenylene vinylene] (MEH-PPV) polymer covered by silica nanoshells synthesized from a sol–gel process was investigated. The optical properties of the samples at different physicochemical conditions were investigated. In contrast to the previous works,[14–16] the results present relatively major changes in the position and shape of the PL peaks as well as in the frequency of the main Raman vibrational modes, as discussed in the Results and Discussion section. All energy shifts observed in the different samples can be correlated to effects of the packing conditions of the MEH-PPV molecules inside the silica nanoshells, which follow the same trends of pressure effects in polymer solutions. Our final remarks and perspectives are described in the conclusions.

MATERIALS AND METHODS

The sol–gel silica nanoparticles were synthesized as follows. First, tetraethylorthosilicate (TEOS), sodium dodecylsulfate (SDS), and ditridecylamine (DTDA) were mixed. A 1 : 1 SDS/DTDA molecular ratio and a 5 : 1 TEOS/DTDA volume ratio were used. Next, MEH-PPV (obtained from Sigma-Aldrich) was dissolved in chloroform ($CHCl_3$) to form a saturated solution and was dropwisely added into the TEOS/SDS/DTDA mixture. The solution immediately turned from orange to red. Deionized water was then added to the solution, H_2O/TEOS volume ratio 2 : 1. The final solution was sonicated and agitated alternately in successive cycles of 5 min for 4 h. The final product turned out to be a dark pink aqueous suspension.

Afterwards, the mean hydrodynamic diameter of the particle in suspension was measured using a dynamic light scattering apparatus.

Subsequently, the suspension was either freeze-dried or heat-dried (50°C) in vacuum. Freeze-drying was done in a commercial lyophilizer by fast-freezing in liquid nitrogen, which prevents water to crystallize inside the silica and break the formed silica nanoshell. The sample was then put inside a vacuum chamber were it remained for 24 h.

Heat-drying was done in a commercial oven under vacuum for 24 h. The final vacuum in both cases was in the range of 10^{-3} Torr. The freeze-dried sample was light pink fine powder, while the heat-dried sample was redder coarse grains. Leaching tests were conducted on both samples.

Scanning electron microscopy (SEM) of the freeze-dried and heat-dried samples was done using the following procedure. The glass substrates were covered with a thin layer (1 nm) of sputtered gold in vacuum. The samples were then deposited on the metal side of the substrates and put under vacuum at room temperature.

Nitrogen adsorption–desorption isotherms of the freeze-dried sample were measured and Brunauer–Emett–Teller theory (BET) along with Barret–Joyner–Hallenda calculations (BJH) were used to obtain the pore size distribution.

The PL spectra of the aqueous suspension, freeze-dried, heat-dried, and the rehydrated freeze-dried samples were measured at room temperature. The freeze-dried sample was also rehydrated to verify the reversibility of the dehydration and the PL spectra was measured again. The PL spectra were obtained with the samples under a He-atmosphere inside an immersion cryostat, to avoid any photooxidation effect. A CW Ar-ion laser emitting at 488 nm, which is near the absorption maximum of MEH-PPV, was used as the excitation source. The PL emission was collected from the samples at a 45° configuration, focused into a SPEX 0.75 m monochromator, and detected using a gallium arsenide (GaAs) photomultiplier tube.

The Raman measurements of the aqueous suspension, heat-dried, and freeze-dried samples were performed in a Jobin-Yvon Raman system, model LABRAM 800, equipped with a cooled charge-coupled device detector. The spectra were collected in a backscattering configuration by a microscope using different (10×, 50×, and 100×) objectives. The 632.8 nm line from a He–Ne laser was used as the excitation source.

SAXS measurements were done on the freeze-dried sample. X-ray scattering experiments were carried out on solid powders in 1-mm diameter glass capillaries. We worked in a transmission configuration. A copper rotating anode X-ray source with a multilayer focusing ''Osmic'' monochromator giving high flux (10^8 photons/s) and punctual collimation was employed. Scattered intensity was measured by an ''Image plate'' 2D detector. X-ray scattering patterns were obtained giving the scattered intensity as a function of the wave vector q (nm^{-1}). Scattering intensity was corrected by scattered and transmitted intensity from an empty capillary.

RESULTS AND DISCUSSIONS

The dynamic light scattering apparatus measured a particle mean hydrodynamic diameter of 360 nm with 13% of polydispersion in the aqueous suspension.

Both freeze-dried and heat-dried samples were subjected to leaching of MEH-PPV in $CHCl_3$. The freeze-dried sample leached completely in a few minutes while the heat-dried sample took several hours for leaching completely.

SEM images of the heat-dried and freeze-dried samples are shown in Figure 1. Films made from the resuspended freeze-dried sample in water show typical clay-like characteristics. Heat-dried films show

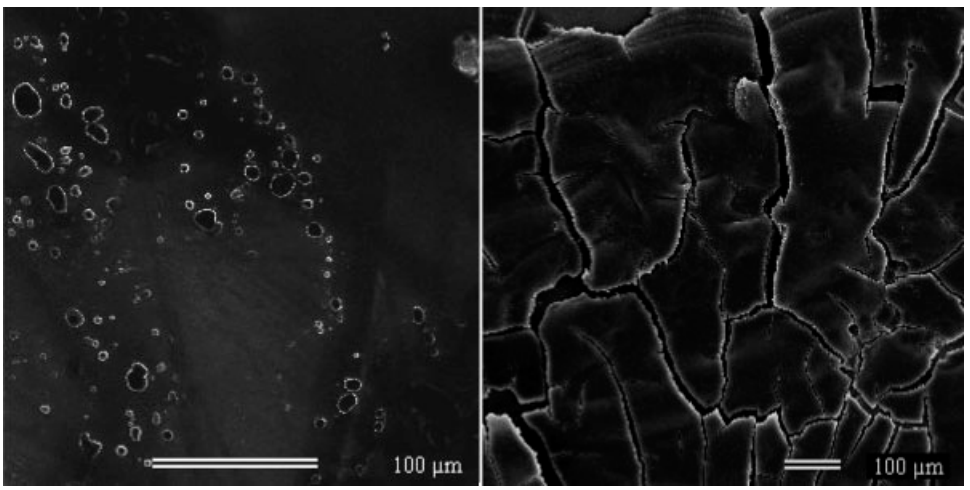

Figure 1 SEM of heat-dried sample (left) and freeze-dried sample (right) spread over the metallic substrate side.

micrometric globules with a large size distribution but also present macroscopic pieces with irregular shape.

The results of nitrogen adsorption–desorption experiments are shown in Figure 2.

BET–BJH calculations show that there is a large distribution of ''pore'' diameters in the freeze-dried samples. It is worth to emphasize that BET–BJH cannot distinguish between ''inner'' and ''outer'' surfaces. It means that the nanoshell outer surface is taken into account when pores are being counted. However, dynamic light scattering shows a mean diameter for the particles in the suspension that is at least twice the value of the largest ''pore'' calculated by BET–BJH of the freeze-dried samples. Gel shrinkage upon drying is a well-known phenomenon.[19] It is reasonable to suppose that the freeze-dried samples present a mean nanoshell diameter smaller than the mean diameter originally present in the suspension, as a result of the drying process.

Together, the leaching experiment, the nitrogen adsorption–desorption experiment and the dynamic light scattering, as well as the clay-like characteristics of the SEM of the freeze-dried sample (powder), show that the material is a nanostructured formation with pores.

The resulting sonicated nanostructured siliceous powder from the mixture of MEH-PPV/$CHCl_3$/TEOS/SDS/DTDA/H_2O suggests that nanostructured MEH-PPV surfacted by both SDS and DTDA forms a template for silica deposition from TEOS hydrolysis. The formation of the nanostructured MEH-PPV occurs possibly during the visual color changes from orange to red when the saturated MEH-PPV–$CHCl_3$ solution was dropwisely added into the TEOS/SDS/DTDA mixture.

Moreover, according to dynamic light scattering, the suspension presents a narrower distribution in diameter than that of the freeze-dried sample pores (data not shown). Proportional shrinkage of pores would make the distribution of pores narrower. In other words, one would expect the large distribution of pores accounted by BET–BJH to be even larger in the suspension.

The spectra for the nanostructured suspension, the freeze-dried, and heat-dried samples (Fig. 3) present a relatively large red shift in respect to the spectrum obtained from a solution of MEH-PPV in tetrahydrofuran (THF). The position of the pure electronic transition peaks (00 peaks) for each case is 593, 600, and 609 nm, respectively. The first vibronic band (01 peak) situated at around 640 nm increases in intensity from the suspension to the heat-dried case, while a shoulder situated below 570 nm diminishes.

The presence of the shoulder below 570 nm, not observed in the spectrum of MEH-PPV in THF solution, can be related to an emission process from MEH-PPV molecular segments inside the silica nanoshells that have lower conjugation lengths, and/or could be

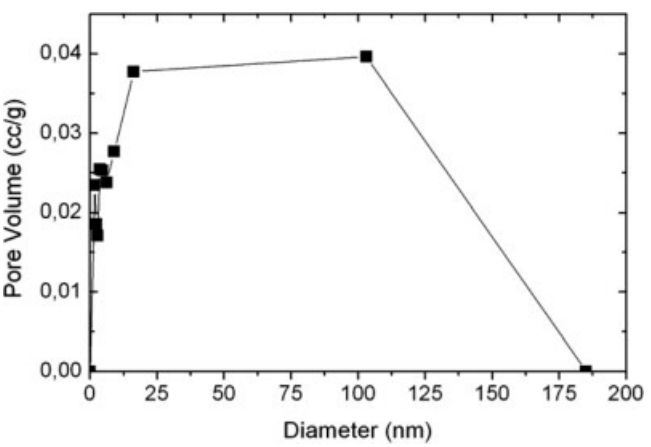

Figure 2 BET–BJH desorption pore size distribution of the freeze-dried sample.

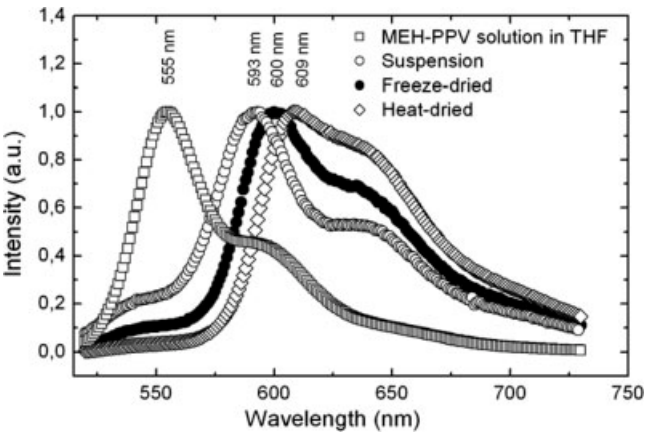

Figure 3 PL spectra of the nanostructured suspension, the freeze-dried, and the heat-dried samples. The spectrum of the MEH-PPV in solution of THF is used as a reference. The spectra were normalized for a better comparison.

due to optical processes (scattering, luminescence) involving the remainders of the compounds which did not participate in the silica nanoshells formation, i.e., TEOS, SDS, and DTDA. Although both interpretations are possible, the latter should be the main reason because the shoulder intensity is higher in the suspension correlating to a higher volume fraction of unused TEOS, SDS, and DTDA. The freeze-drying process should remove at least part of the unused TEOS, SDS, and DTDA with the water evaporation. One expects that the heat-drying process will remove a larger fraction of the same compounds. This corresponds to the behavior of the shoulder intensity, as observed in Figure 3.

Figure 4 shows the spectra of the suspension, the freeze-dried, and the rehydrated freeze-dried samples. It is worth noticing that the PL spectrum of the rehydrated freeze-dried sample matches well in shape with that of the suspension. The only differences are the relative small shift of 1 nm between them and the reduction in the relative intensity for the shoulder below 570 nm. This demonstrates that the surfacted MEH-PPV inside the silica nanoshells in the rehydrated freeze-dried sample recuperates the same physical conditions that it has in the suspension.

For the freeze-dried sample, great part of the unused TEOS, SDS, and DTDA evaporated during the drying process. By adding water, the nanoshells are simply rehydrated, without change in the amount of TEOS/SDS/DTDA. This would explain the same shoulder intensity for freeze-dried and rehydrated freeze-dried samples, and would reinforce the interpretation that the TEOS/SDS/DTDA mixture is responsible for the shoulder emission.

The difference in shape (different Huang–Rhys factors) and the relative 00 peak energy shift of 6 nm between the PL spectra of freeze-dried and rehydrated freeze-dried samples (Fig. 4) have a qualitative explanation similar to that given when PL emission from solid state films and solutions of conjugated polymers are compared.[20]

The red shifts of the suspension, the heat-dried, and the freeze-dried samples, relative to the reference spectrum (Fig. 3), are 0.143, 0.168, and 0.198 eV, respectively. It is worth noting that with the increase in the red-shift energy, the Huang–Rhys factor (S), which is evaluated from the intensity of the first 01 vibronic transition relative to the 00 transition, also increases. Smaller S values correspond to a more clear vibrational structure, which in turn correspond to a higher structural ordering of the polymeric system.[21] The PL red-shift effect, followed by an increase of the Huang–Rhys factor, was reported by Ruseckas et al. for different types of polythiophenes films.[22] They observed a PL red shift of 0.170 eV for the polythiophene with smaller side-groups relative to a sample with higher side-groups. Smaller side-groups corresponds to a smaller interchain distance, and therefore, to a denser chain packing. They attributed the red shift to a more efficient trapping of intrachain excitons into aggregate sites due to the higher interchain interaction; the red-shift value being an estimative of the strength of the interchain interaction in the aggregate. As the density of intrachain excitons trapped into the aggregate increases, electrons will become more localized and thus a higher interaction between them and the vibrational modes of the polymeric molecules is expected. This will lead to higher vibronic bands, resulting in higher Huang–Rhys factors, as observed in Ref. [22] and in this work.

The packing conditions of the MEH-PPV molecules inside the silica nanoshells constitute a reasonable explanation for the resulting PL spectra of our samples. The observed red-shift values are of the same order as that reported for polythiophene samples.[22] They

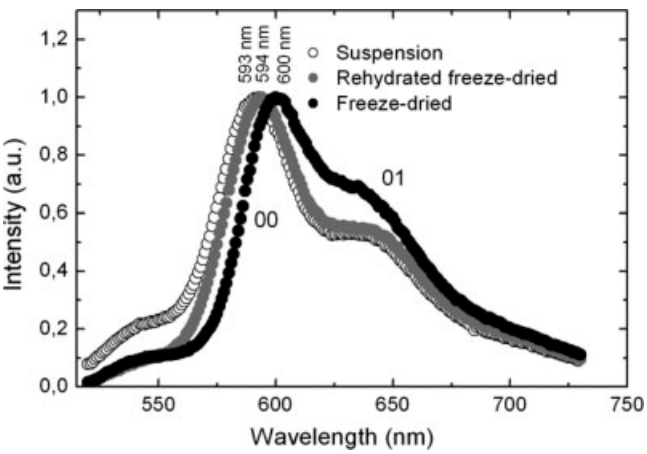

Figure 4 PL spectra of the nanostructured suspension, the freeze-dried, and the rehydrated freeze-dried samples at room temperature. The normalization of the spectra was performed for better comparison.

increase concomitantly with the Huang–Rhys factor from the suspension to the heat-dried case (Fig. 3). The Huang–Rhys factor for the suspension spectrum is slightly higher than that for the reference spectrum; however, it is significantly higher for the heat-dried and the freeze-dried samples. When the silica nanoshell is formed around the surfacted MEH-PPV, their pores are filled with water. During the freeze and heat drying process, water leaves the nanoshell pores causing the nanoshell to shrink, which enables the surfactant molecules to enter the empty pores to minimize their free energy. The packing force exerted on the inner core of MEH-PPV is expected to increase. Thus, the heat-dried and the freeze-dried cases would correspond to a denser packing condition of the MEH-PPV molecules, with a higher probability to form aggregates, and thus favoring a higher interchain interaction.

It is worth mentioning that packing and pressure effects are similar in conjugated polymers and should present the same trends on their optical properties. The pressure applied by the shrunk nanoshells would compress the polymer molecules, increasing effectively the concentration of the molecules surrounding any photogenerated exciton, and therefore, enhancing any environmental contribution to the exciton energy. Pressure effects reported on PPV[23] and on MEH-PPV[24] show similarly red shifts of the PL emission and a decrease of the PL intensity, together with the increase of the Huang–Rhys factor. One of the most significant effects of increasing the concentration of the material (due to packing conditions or applied pressure) surrounding an exciton is expected to be the ''gas-to-crystal'' shift.[25–29] This corresponds to the lowering of the exciton energy as a result of the polarization of the surrounding medium. In this work, this effect would be caused by the aggregation of neighboring polymer molecules inside the silica nanoshells and would be even higher when induced by the drying process.

Pressure effects cause the vibrational modes of PPV[23,30] to have higher frequencies. Assuming that the enhancement of the packing effect of MEH-PPV molecules inside the silica nanoshells will follow the trends of the pressure effect, one would observe an increase in the frequency of the vibrational modes for the heat-dried and the freeze-dried cases in comparison to the suspension sample.

The Raman spectra for the three samples are shown in Figure 5(a). Figure 5(b) depicts only the more intense Raman line observed around 1580 cm^{-1}.

The arrows in Figure 5(a) indicate the most intense vibrational modes of the MEH-PPV conjugated polymer.[31] The Raman band observed at 1450 cm^{-1} corresponds to a vibrational mode from TEOS related to C—H stretching,[32] and the Raman line around 1580 cm^{-1} is associated to the C—C stretching of the

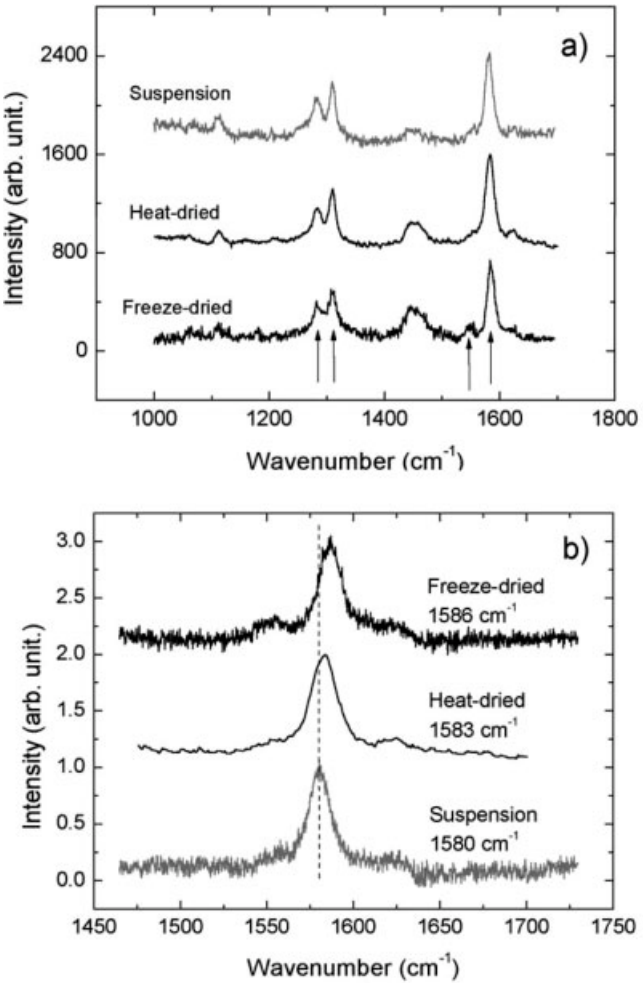

Figure 5 (a) Raman spectra of the suspension, the freeze-dried, and the heat-dried samples at room temperature and (b) the more pronounced Raman line at around 1580 cm^{-1} for the same samples. The spectra in both figures were normalized and shifted in the *y*-axis for clarity.

phenyl ring[31,33] for PPV and other PPV derivatives. This line presents the expected displacement to higher frequencies for the heat-dried and the freeze-dried samples, in agreement to the assumption that the MEH-PPV molecules are in denser packing conditions. However, for the heat-dried sample this line presents a relative displacement of 3 cm^{-1}, which is lower than the relative displacement of 6 cm^{-1} observed for the freeze-dried case. This does not correspond to the respective progression of the PL red shift observed in Figure 3. On the other hand, the higher temperature during the heat drying process could also induce a higher aggregation between the MEH-PPV molecules, leading to an additional PL red shift, but not affecting effectively the electron interaction with the vibrational mode.

The high polarity solvents that are capable of forming hydrogen bonding can cause PL spectral shift.[34] However, the comparison between the MEH-PPV PL spectra in different solvents, for example, the spectra

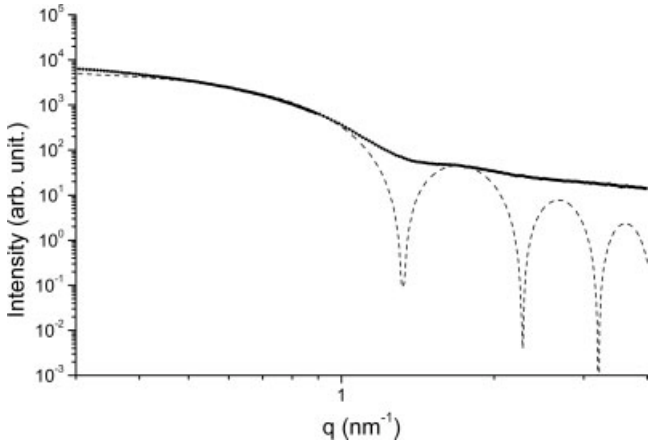

Figure 6 SAXS of the rehydrated freeze-dried sample. The dashed line is a model for a compact spherical particle of 7 nm (diameter).

of MEH-PPV in chloroform, a high polarity solvent (data not shown), and toluene, a low polarity solvent,[35] both show a shift smaller than the one observed in our results (Fig. 3). Moreover, DTDA is most probably interfacing MEH-PPV and silica, with the amine group facing the silica and the alkyl group facing the MEH-PPV for energy minimization, which can prevent hydrogen bond interactions between MEH-PPV and silica or MEH-PPV and water.

The most important point is that the PL and Raman results qualitatively confirm the expected trends due to the more dense packing effects exerted by the silica nanoshell covering the MEH-PPV. The results observed for the rehydrated freeze-dried sample (Fig. 4) also favor the explanations based on the packing effect, since the addition of water would relax the surrounding molecules leading to the prior packing conditions of the suspension sample.

SAXS measurements are shown in Figure 6 along with a model of a compact spherical particle scattering. A mean diameter of 7 nm is found. A slight broadening (0.8 nm) of the distribution in particle size can enhance the fitting (not shown), but the model is enough to determine the mean diameter. Particle size above 7 nm is not found, mainly because the silica shell X-ray scattering obliterates the inner core of MEH-PPV. The X-ray scattering power of silicon is far greater than the scattering power of carbon. In addition, the concentration by weight of MEH-PPV is 100 times smaller than that of silica. It means that the SAXS experiment is probing only the nanoparticles of the silica gel that form the nanoshells and the size of the MEH-PPV core is not accessible by SAXS.

CONCLUSIONS

In summary, we present a sol–gel process in which MEH-PPV was covered by silica nanoshells resulting in an aqueous suspension. The silica nanoshells present diameter and pore size in the nanometric range. Leaching of the MEH-PPV from the silica nanoshells is possible with chloroform addition depending on the drying process. From the suspension to the heat-dried samples the emission properties of the MEH-PPV presented a large red shift of the 00 peak energy, followed by an increase of the Huang–Rhys factor in comparison to the MEH-PPV in THF reference solution. The more pronounced Raman line at 1580 cm^{-1} is displaced to higher frequencies for the heat-dried and the freeze-dried samples, as expected from a denser packing condition. The PL results for the rehydration of the freeze-dried sample have also shown that packed MEH-PPV molecules can be relaxed, recuperating the same packing conditions of the initial suspension. All these results are in conformity with the interpretation that packing effects inside the silica nanoshells are inducing the formation of aggregates in which there is a higher probability of interchain interactions.

We thank Luis Rodrigues Armoa Garcia and Estefânia Mara do Nascimento (CDTN/CNEN) for the Scanning Electron Microscopies and BET measurements, Alvaro V. Teixeira for helping in the dynamic light scattering measurements, and the Metallurgical Engineering Department of UFMG for permitting the use of its Raman facilities. SEM and SEM-microprobe analysis were performed at LMA (Laboratório de Microanálise) of Física-Geologia-Química/UFMG—CDTN/CNEN Consorptium. We also thank Rogério Zadra (BASF-Brasil) for supplying DTDA.

References

1. Friend, R. H.; Gymer, R. W.; Holmes, A. B.; Burroughes, J. H.; Marks, R. N.; Talian, C.; Bradley, D. D. C.; dos Santos, D. A.; Brédas, J. L.; Lodlung, M.; Salaneck, W. R. Nature 1999, 397, 121.
2. Hide, F.; Díaz-García, M. A.; Schwartz, B. J.; Heeger, A. J. Acct Chem Res 1997, 30, 430.
3. Rothberg, L. J.; Lovinger, A. J. J Mater Res 1996, 11, 3174.
4. Carter, S. A.; Scott, J. C.; Brock, P. J. Appl Phys Lett 1997, 71, 1145.
5. Hide, F.; Schwartz, B. J.; Díaz-García, M. A.; Heeger, A. J. J Chem Phys Lett 1996, 256, 424.
6. Greenham, N. C.; Xiaogang, P.; Alivisatos, A. P. Phys Rev B 1996, 54, 17628.
7. Gao, G. Y.; Hummelen, J. C.; Wudl, F.; Heeger, A. J. Science 1995, 270, 1789.
8. Kim, H.; Kim, J. Y.; Lee, K.; Park, Y.; Jin, Y.; Suh, H. Appl Phys 2001, 1, 139.
9. Lin, H.; Weng, Y.; Huang, H.; He, Q.; Zheng, M.; Bai, F. Appl Phys Lett 2004, 84, 2980.
10. Breeze, A. J.; Schlesinger, Z.; Carter, S. A.; Brock, P. J. Phys Rev B 2001, 64, 125205.
11. Slooff, L. H.; Wienk, M. M.; Kroon, J. M. Thin Solid Films 2004, 451, 634.
12. Sarathy, K. V.; Narayan, K. S.; Kim, J.; White, J. O. Chem Phys Lett 2000, 318, 543.
13. Cury, L. A.; Ladeira, L. O.; Righi, A. Synth Met 2003, 139, 283.
14. Nguyen, T. P.; Lakehal, M.; Le Rendu, P.; Joubert, P.; Destruel, P. Synth Met 2000, 111–112, 199–202, .

15. Ho, P. K. H.; Kim, J.-S.; Tessler, N.; Friend, R. H. J Chem Phys 2001, 115, 2709.
16. Lim, Y. T.; Lee, T.-W.; Lee, H.-C.; Ok Park, O. Synth Met 2002, 128, 133.
17. Schwartz, B. J.; Nguyen, T.-Q.; Wu, J.; Tolbert, S. H. Synth Met 2001, 116, 35.
18. Wu, J.; Gross, A. F.; Tolbert, S. H. J Phys Chem B 1999, 103, 2374.
19. Smith, D. M.; Scherer, G. W.; Anderson, J. M. J Non-Cryst Sol 1995, 188, 191.
20. Gettinger, C. L.; Heeger, A. J.; Drake, J. M.; Pine, D. J. J Chem Phys 1994, 101, 1673.
21. Pichler, K.; Halliday, D. A.; Bradley, D. D. C.; Burn, P. L.; Friend, R. H.; Holmes, A. B. J Phys Condens Matter 1993, 5, 7155.
22. Ruseckas, A.; Namdas, E. B.; Ganguly, T.; Theander, M.; Svensson, M.; Anderson, M. R.; Inganas, O.; Sundstrom, V. J Phys Chem B 2001 2001, 7624.
23. Webster, S.; Batchelder, D. N. Polymer 1996, 37, 4961.
24. Tikhoplav, R. K.; Hess, B. C. Synth Met 1999, 101, 236.
25. Rice, S. A.; Jortner, J. J. In Physics of Solids at High Pressure; Tomizuka, C. T., Enrick, R. M. Eds. London: Academic Press, 1965.
26. Lochner, K.; Bassler, H.; Sowa, H.; Ahgbahs, H. Chem Phys 1980, 52, 179.
27. Webster, S.; Batchelder, D. N. Macromol Symp 1994, 87, 177.
28. Lacey, R. J.; Batchelder, D. N.; Pitt, G. D. J Phys C: Solid State Phys 1984, 17, 4529.
29. Longuet-Higgins, H. C.; Pope, J. A. J Chem Phys 1957, 27, 192.
30. Cottle, A. C.; Lewis, W. F.; Batchelder, D. N. J Phys C: Solid State Phys 1978, 11, 605.
31. Mulazzi, E.; Ripamonti, A.; Wery, J.; Dulieu, B.; Lefrant, S. Phys Rev B 1999, 60, 16519.
32. Matos, M. C.; Ilharco, L. M.; Almeida, R. M. J Non-Cryst Solids 1992, 147, 232.
33. Oliveira, F. A. C.; Cury, L. A.; Righi, A.; Moreira, R. L.; Guimarães, P. S. S.; Matinaga, F. M.; Pimenta, M. A.; Nogueira, R. A. J Chem Phys 2003, 119, 9777.
34. Schaller, R. D.; Lee, L. F.; Johnson, J. C.; Haber, L. H.; Saykally, R. J.; Vieceli, J.; Benjamin, I.; Nguyen, T.-Q.; Schwartz, B. J. J Phys Chem B 2002, 106, 9496.
35. Traiphol, R.; Sanguansat, P.; Srikhirin, T.; Kerdcharoen, T.; Osotchan, T. Macromolecules 2006, 39, 1165.